Stable Frank–Kasper phases of self-assembled, soft matter spheres

Abhiram Reddy[a], Michael B. Buckley[b], Akash Arora[c], Frank S. Bates[c,1], Kevin D. Dorfman[c,1], and Gregory M. Grason[a,1]

[a]Department of Polymer Science and Engineering, University of Massachusetts, Amherst, MA 01003; [b]Department of Physics, University of Massachusetts, Amherst, MA 01003; and [c]Department of Chemical Engineering and Materials Science, University of Minnesota, Minneapolis, MN 55455

Contributed by Frank S. Bates, August 6, 2018 (sent for review June 5, 2018; reviewed by Scott Milner and Gerd Schroeder-Turk)

Single molecular species can self-assemble into Frank–Kasper (FK) phases, finite approximants of dodecagonal quasicrystals, defying intuitive notions that thermodynamic ground states are maximally symmetric. FK phases are speculated to emerge as the minimal-distortional packings of space-filling spherical domains, but a precise measure of this distortion and how it affects assembly thermodynamics remains ambiguous. We use two complementary approaches to demonstrate that the principles driving FK lattice formation in diblock copolymers emerge directly from the strong-stretching theory of spherical domains, in which a minimal interblock area competes with a minimal stretching of space-filling chains. The relative stability of FK lattices is studied first using a diblock foam model with unconstrained particle volumes and shapes, which correctly predicts not only the equilibrium σ lattice but also the unequal volumes of the equilibrium domains. We then provide a molecular interpretation for these results via self-consistent field theory, illuminating how molecular stiffness increases the sensitivity of the intradomain chain configurations and the asymmetry of local domain packing. These findings shed light on the role of volume exchange on the formation of distinct FK phases in copolymers and suggest a paradigm for formation of FK phases in soft matter systems in which unequal domain volumes are selected by the thermodynamic competition between distinct measures of shape asymmetry.

self-assembly | Frank–Kasper phases | optimal lattices | block copolymers

Spherical assemblies occur in nearly every class of supramolecular soft matter, from lyotropic liquid crystals and surfactants to amphiphillic copolymers (1). In concentrated or neat systems, self-assembled spherical domains behave as giant "mesoatoms," adopting periodically ordered crystalline arrangements. While superficially similar to lattices formed in atomic or colloidal systems—which are stabilized largely by bonding or translational entropy—the periodic order in soft materials is governed by distinctly different principles because lattice formation occurs in thermodynamic equilibrium with the formation of the mesoatoms from the constituent molecules themselves. Thus, the equilibrium sizes and shapes of mesoatoms are inextricably coupled to the lattice symmetry and vice versa.

In this article, we address the emergence of noncanonical, Frank–Kasper (FK) lattices in soft materials, characterized by complex and large unit cells yet formed by assembly of a single molecular component. Initially constructed as models of metallic alloys (2, 3), FK lattices are a family of periodic packings (4, 5) whose sites are tetrahedrally close packed (i.e., sitting on the vertices of nearly equilateral tetrahedra, the densest local arrangement of equal radius spheres) and can be decomposed into polyhedral (e.g., Voronoi or Wigner Seitz) cells surrounding each site containing 12, 14, 15, or 16 faces. Known as the FK polyhedra, these cells (Z12, Z14, Z15, and Z16) possess variable volume and envelope spheres of distinct radii. Hence, FK lattices are natural candidates to describe ordered, locally dense packings of spherical elements of different radii such as atomic alloys (3, 5) or binary nanoparticle superlattices (6). Once considered anomalous in soft matter systems, the past decade has seen an explosion in the observation of FK lattices in a diverse range of sphere-forming assemblies. These include (A15, σ) liquid–crystalline dendrimers (7, 8), (A15, σ) linear tetrablock (9, 10), (σ, C14, C15) diblock (11–13) and (A15) linear–dendron (14) block copolymer melts, (A15) amphiphilic nanotetrahedra (15, 16), (A15, σ, C14, C15) concentrated ionic surfactants (17, 18), and (C14) monodisperse, functionalized nanoparticles (19). The central puzzle surrounding the formation of FK lattices in these diverse systems is understanding why single components assemble into phases composed of highly heterogeneous molecular environments.

A common element distinct to FK formation in soft systems is the thermodynamic cost of asphericity imposed by incompatibility between uniform density and packing of perfectly spherical objects (Fig. 1). In soft assemblies, the ideally spherically symmetric domains are warped into lower symmetry, polyhedral shapes that fill space without gaps. Intuitively, one expects that the minimal free-energy state is the one for which the quasi-spherical domains (qSDs) remain "most spherical." The most commonly invoked notion of sphericity in this context is the dimensionless cell area A to volume V ratio, $\mathcal{A} \equiv A/(36\pi V^2)^{1/3}$, which has a lower bound of 1 achieved by perfect spheres. The cellular partitions of FK lattices play a key role in the mathematical modeling of dry foams, known

Significance

Formation of complex Frank–Kasper phases in soft matter systems confounds intuitive notions that equilibrium states achieve maximal symmetry, owing to an unavoidable conflict between shape and volume asymmetry in space-filling packings of spherical domains. Here we show the structure and thermodynamics of these complex phases can be understood from the generalization of two classic problems in discrete geometry: the Kelvin and Quantizer problems. We find that self-organized asymmetry of Frank–Kasper phases in diblock copolymers emerges from the optimal relaxation of cellular domains to unequal volumes to simultaneously minimize area and maximize compactness of cells, highlighting an important connection between crystal structures in condensed matter and optimal lattices in discrete geometry.

Author contributions: A.R., M.B.B., A.A., F.S.B., K.D.D., and G.M.G. designed research; A.R., M.B.B., A.A., and G.M.G. performed research; A.R., M.B.B., A.A., and G.M.G. analyzed data; and A.R., F.S.B., K.D.D., and G.M.G. wrote the paper.

Reviewers: S.M., The Pennsylvania State University; and G.S.-T., Murdoch University, Australia.

The authors declare no conflicts of interest.

[1]To whom correspondence may be addressed. Email: grason@mail.pse.umass.edu, dorfman@umn.edu, or bates001@umn.edu.

This article contains supporting information online at www.pnas.org/lookup/suppl/doi:10.1073/pnas.1809655115/-/DCSupplemental.

Published online September 24, 2018.

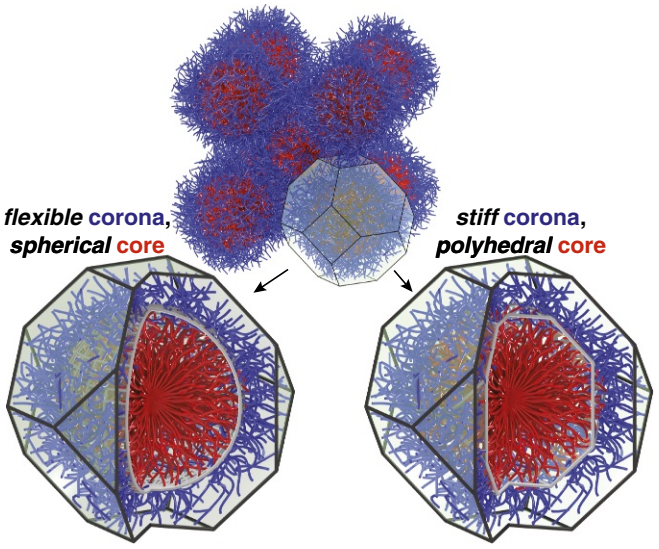

Fig. 1. Chain packing of spherical diblock copolymer domains of the BCC lattice (*Top*), with corresponding limits of weakly coupled (*Bottom Left*) and strongly coupled (*Bottom Right*) of core domain shape of polyhedral (truncated-octohedron) cell symmetry.

as the Kelvin problem (20–23), which seeks minimal area of partitions of space into equal volume cells.* Based on the fact that the lowest area, equal-volume cellular partition known to date, the Weaire–Phelan foam (20), derives from the FK lattice A15, Ziherl and Kamien proposed that this lattice is generically favored thermodynamically in so-called "fuzzy colloid" models (24, 25), an argument subsequently adapted to sphere phases of block copolymers (26, 27). Recently, Lee, Leighton, and Bates (11) reasoned that average "sphericity" could be increased (i.e., decreased mean $\mathcal{A}$) below the Weaire–Phelan structure if the equal-volume constraint for distinct cells is relaxed, as would occur for molecular exchange between distinct qSDs, presumably in equilibrium with the thermodynamic cost for deviations from a preferred aggregation number. Based on the Voronoi partitions, which have unequal volumes for FK lattices, σ was argued to have a lower mean dimensionless area than A15 and thus should be stable over that lattice according to the sphericity argument, consistent with observations of a σ lattice in diblock copolymer melts (13) and self-consistent field theory (SCFT) of conformationally and architecturally asymmetric diblocks (28).

While the role of volume asymmetry has been implicated previously in the formation of FK lattices by soft qSD assemblies (29), critical questions remain unanswered. First, what are the relevant measures of sphericity optimized by the assembly thermodynamics? Second, how do these in concert determine the optimal balance between shape asymmetry (nonspherical domains) and volume asymmetry (molecular partitioning among domains) for a given qSD lattice? Finally, how does this balance select the equilibrium lattice and determine the scale of thermodynamic separation between the many competing FK lattices? We address these questions in the context of what we call the diblock foam model (DFM), which describes the thermodynamic competition between interdomain surface energy and chain stretching. For optimal mean qSD size, the DFM quantifies the thermodynamic cost of asphericity in terms of a geometric mean of reduced cell area and dimensionless radius of gyration of the cells and thus integrates elements of both the Kelvin and lattice Quantizer problems (30). These geometric proxies for interblock repulsion and intramolecular stretching in qSD exhibit qualitatively different dependencies on cell shape, a factor that we show, based on this model and SCFT analysis, to be critical to the volume partitioning among distinct qSD and optimal lattice selection.

Among the various classes of FK-forming soft matter (7–9, 11–15, 17, 19), we posit that diblock copolymers represent the optimal starting point for investigating the selection of low-symmetry FK phases by soft matter spheres. Diblock copolymers are a relatively simple chemical system, consisting of two flexible chains bonded together at their ends, and there exist robust theoretical methods for studying their phase behavior in the context of universal physical models (31, 32). The fundamental mechanisms underlying assembly of diblock copolymers that we elucidate here furnish the foundation for subsequent investigations of other soft matter systems, where these basic principles are conflated with additional phenomena emerging from electrostatics, hydrophobic interactions, and detailed packing of the complicated (non-Gaussian) configurations of their constituents.

DFM of FK Lattice Selection

We adopt what we call the DFM, first developed by Milner and Olmsted (33, 34), in which the free energy of competing arrangements is reduced to purely geometric measures of the cellular volumes enclosing the qSD. To a first approximation, these cells are the polyhedral Voronoi cells for a given point packing, whose faces represent coronal brushes flattened by contact with neighboring qSD coronae. The model is based on strong-stretching theory (SST) of diblock copolymer melts, in which interblock repulsions drive separation into sharply divided core and coronal domains and the chains are well-extended. We also consider the case of large elastic asymmetry between core and coronal blocks, which itself derives from asymmetry of the block architecture or the segment sizes. This corresponds to the polyhedral-interface limit (35), in which the core/coronal interface in each qSD adopts a perfect, affinely shrunk copy of the cell shape (see Fig. 1, *Bottom Right*). Polyhedral warping of the interface is favored when the stiffness of the coronal blocks, which favors a more uniform extension from the interface to the outer cell wall, dominates over entropic stiffness of core blocks and interblock surface energy, both of which favor round interfaces.

In this limit, the free energy per chain (26, 34), $F(X)$, of a given lattice packing X derives from two contributions,

$$F(X)=\gamma\frac{\mathcal{A}(X)}{R_0}+\frac{\kappa}{2}\mathcal{I}(X)R_0^2, \qquad [1]$$

where γ and κ are coefficients fixed by the chain properties (i.e., block lengths, segment lengths, interblock repulsion), and R_0 is the radius of a sphere of equal volume to the mean volume of cells, or $(4\pi/3)R_0^3=n_X^{-1}\sum_{i=1}^{n_X}V_i$, where V_i is i^{th} cell volume of n_X total cells in X (see *SI Appendix*, *1A*. Polyhedral Interface Limit of Strongly-Segregated Diblock Sphere Lattices for details). The first term represents the enthalpy of core–corona contact and hence is proportional to the (per volume) interfacial area, which itself is proportional to the cell area A_i, measured by the dimensionless (mean) cell area, $\mathcal{A}(X)=(n_X^{-1}\sum_{i=1}^{n_X}A_i)/(4\pi R_0^2)$. The second term represents the entropic cost of extending polymeric blocks (here modeled as Gaussian chains) in radial trajectories within qSD. This cost grows with the square of domain size and depends on qSD shape through the dimensionless square radius of gyration, or

*The tetrahedral coordination of FK lattices implies that their partitions closely approximate the geometric constraints of Plateau borders and are therefore near to minimal-area partitions. In addition to A15, at least two more partitions of FK lattices, σ and H, have also been shown previously (21, 23) to beat the area of optimum originally conjectured by Kelvin, the BCC partition. In *SI Appendix*, *2B*. Minimal Area Cells: Kelvin Problem, we report that the FK lattice P also belongs to this category.

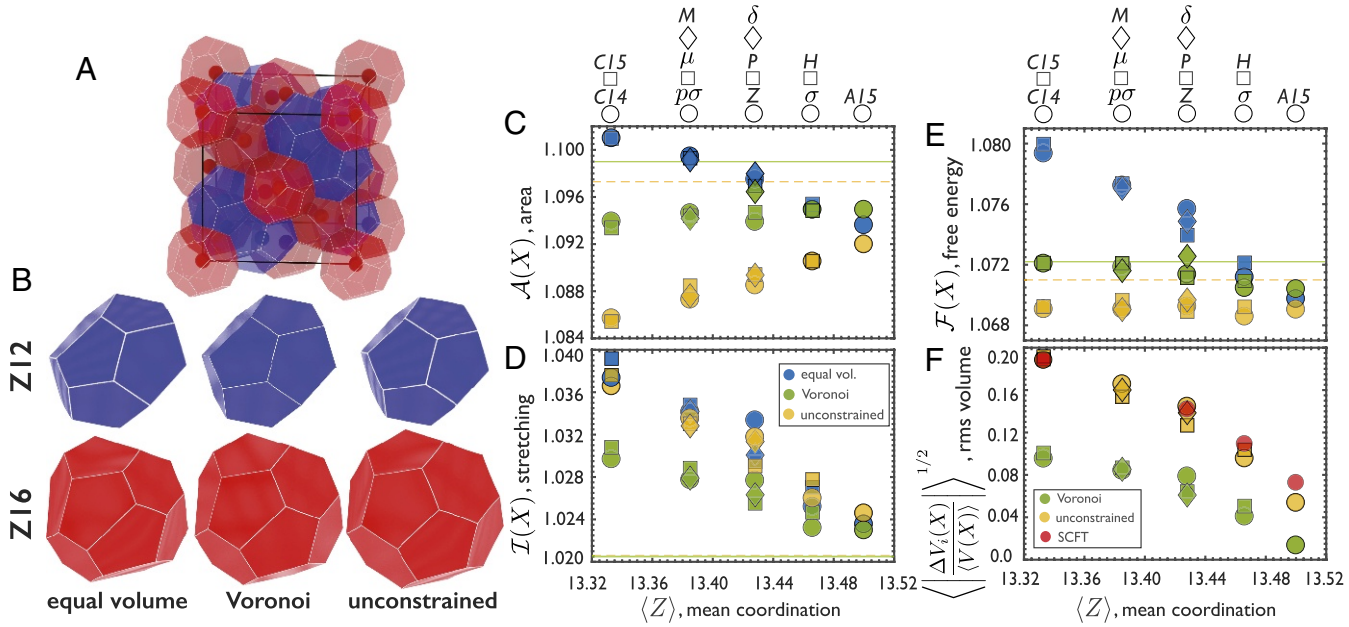

Fig. 2. A DFM structure for the cubic repeat of C15 is shown in *A*, with qSD centers shown within the Z12 and Z16 cells as red and blue, respectively. (*B*) Equilibrium shapes for three cell geometries studied, in which the slight curvature of cell faces and edges is visible for the relaxed shape cases. Results of the DFM are shown for 11 competing FK phases (labeled above), plotted as a function of mean coordination, or average number of cell faces $\langle Z \rangle$: (*C*) mean dimensionless area, (*D*) mean dimensionless stretching, (*E*) mean free energy, and (*F*) rms volume variation among cells relative to mean volume $\langle V(X) \rangle$. In *C*–*E*, points are labeled according to the legend in *D*, and the dashed and solid lines show unconstrained and Voronoi results, respectively, for BCC. In *F*, variable volume cell results are compared with qSD volumes extracted from SCFT at $\chi N = 40$, $f = 0.25$, and $\epsilon = 2$ as described in the text.

stretching moment $\mathcal{I}(X) = (n_X^{-1} \sum_{i=1}^{n_X} I_i)/(4\pi R_0^5/5)$, where $I_i = \int_{V_i} d^3\mathbf{x}\ |\mathbf{x} - \mathbf{x}_i|^2$ is the second-moment volume of the i^{th} cell, whose center lies at $\mathbf{x}_i$. Optimizing mean cell size (R_0) yields the minimal free energy of lattice X, relative to the perfect sphere free-energy $F_0 = \frac{3}{2}(\gamma^2\kappa)^{1/3}$,

$$\mathcal{F}(X) \equiv \min_{R_0} [F(X)]/F_0 = \left[\mathcal{A}^2(X)\mathcal{I}(X)\right]^{1/3}. \qquad [2]$$

This geometric mean favors simultaneously low values of dimensionless area and stretching.[†] While minimal area partitions (at constant volume) are associated with Kelvin's foam problem, lattice partitions that optimize I_i (at fixed density) are the object of the Quantizer problem (30), which has applications in computer science and signal processing (36).

The Milner and Olmsted model has been studied for flat-faced Voronoi cells of face-centered cubic (FCC), body-centered cubic (BCC), and A15 (27, 34), showing that the latter FK lattice of sphere-forming diblocks is favored over former two canonical packings in the polyhedral interface limit. Here, we analyze a vastly expanded class of 11 FK lattices, possessing up to 56 qSD per periodic repeat. Most critically, we use a Surface Evolver (37)-based approach that minimizes $\mathcal{F}(X)$ over arbitrary volumes and shapes of constituent cells in the DFM structure (see *SI Appendix*, *2* for detailed methods and tabulated results).

To assess the importance of relaxing volume and shape, consider the three distinct ensembles of qSD cells, shown for C15 in Fig. 2 *A* and *B*. We have computed results for equal-volume, relaxed-shape cells, which cannot exchange mass, and centroidal Voronoi cells, which have fixed flat-face shapes but unequal volumes (also fixed). The former ensemble neglects the possibility of mass exchange between micelles, while the second optimizes stretching (36) but is suboptimal in terms of cell area.[‡] Neither model is realistic, but they provide useful points of comparison with the unconstrained, relaxed-volume and shape cells, which strictly minimize $\mathcal{F}(X)$ for given X. Fig. 2*C* shows that allowing both volume and shape to relax leads to a complete inversion of the trend of $\mathcal{A}(X)$ with $\langle Z \rangle$. Importantly, there is also a near degeneracy for the free energy of FK structures in Fig. 2*E*, which all lie within 0.08% in $\mathcal{F}(X)$ (as compared with the relatively large $\approx 1\%$ spread for equal-volume qSD). These results confirm the critical role of volume exchange among asymmetric qSD in the thermodynamics of lattice formation (11, 12). Among these nearly degenerate, fully unconstrained DFM structures, the σ phase overtakes A15 (minimal for fixed, equal volume) as the minimal energy phase (with next lowest energy for P), consistent with its observation upon annealing (11, 13) as well as recent SCFT studies of conformationally asymmetric diblocks (28). Notably, however, in the relaxed-volume and shape DFM, σ possesses neither the minimal area (C14) nor minimal stretching (BCC). Rather, its predicted stability results from the optimal compromise between these competing measures of domain asphericity.

The interplay between area and stretching underlies the emergent asymmetry in equilibrium qSD volumes. Comparing the equal-volume to unconstrained DFM results in Fig. 2 *C* and *D* shows that volume relaxation has a far more significant effect on relaxation of $\mathcal{A}(X)$ than $\mathcal{I}(X)$, which changes little by comparison. Relaxation proceeds for all structures by inflating cells with a relatively larger area and shrinking smaller area cells, restrained only by stretching cost creating highly unequal domain sizes (*SI Appendix*, Fig. S1). Volume exchange for lattices with large proportions of lower area Z12 cells (e.g., C14 and C15) achieve

[†] Assembly thermodynamics depends on the dimensionless ratios of structure-averaged area and stretching of cells, as opposed to averages of dimensionless cell area and stretching.

[‡] Centroidal Voronoi cells have generating points at the centers of volume of the cell and, hence, for a given X minimize the mean-square distance of all points to their corresponding central point (see *SI Appendix*, *2A*. Minimal Stretching Cells: Quantizer Problem for additional details).

relatively large ($\approx 2\%$) drops in $\mathcal{A}(X)$ when compared with the high-$\langle Z\rangle$ end of the spectrum (e.g., $\approx 0.2\%$ for A15).

Cell volume asymmetry in equilibrated DFM structures pushes well beyond that of the "natural" geometry of Voronoi cells, which is strictly optimal for stretching but not for its product with the square of dimensionless area. Fig. 2*F* shows that both unconstrained and Voronoi models of qSD cell geometry exhibit an increase volume dispersion with decreasing mean coordination (or with increasing fraction of Z12s). However, optimal unconstrained DFM cells are nearly twice as polydisperse in volume as the Voronoi distribution. This massive volume asymmetry among qSD (up to $\approx 19\%$ variance for C14 and C15) is driven by a dramatic reduction in interblock contact area, a drive that is ultimately limited by the thermodynamic balance with the entropic (stretching) costs of filling space with qSDs of unequal size. These results imply that structures with a larger equilibrium volume dispersion (such as the lower $\langle Z\rangle$ C14 and C15) are more susceptible to the effects of thermal processing that selectively promote or inhibit chain exchange among equilibrating spheres (12) than phases such as A15, which relax free energy relatively little through volume equilibration.

Previous SCFT studies (12, 28) have shown that the canonical BCC sphere phase is overtaken by a stable σ lattice when the elastic asymmetry, embodied by ratios of statistical segment lengths, $\epsilon \equiv a_A/a_B \gtrsim 1.5$. DFM not only correctly predicts σ as the dominantly stable sphere phase but also does a remarkable job of predicting the relative hierarchy among metastable FK competitors. This is evident in *SI Appendix*, Fig. S16 *A–C*, where we compare the free energies, scaled enthalpies, and entropies for σ, Z, C14, C15, and A15 predicted by the unconstrained cell DFM to AB diblock SCFT calculations using methods described in ref. 32 at somewhat strong segregation conditions $\chi N = 40$, where χ is the Flory–Huggins parameter for A/B contact and N is the degree of polymerization. DFM correctly predicts the narrow 0.01% scale of free-energy splitting between these competitors for $\epsilon = 2$ diblocks in the composition range $f \leq 0.25$, where f is the volume fraction of the minority block. Moreover, DFM predicts their ranking relative to σ with the exception of Z, which DFM predicts to be nearly degenerate with C15. The accuracy of DFM extends beyond thermodynamics to structure, most notably the volume asymmetry in Fig. 2*F*.

Molecular Mechanism of Aspherical Domain Formation

To probe the molecular mechanism that underlies the selection of FK lattices in block copolymers, we analyze two order parameters that quantify the respective asymmetric shapes and volumes of qSD, computed from the volumes enclosing A-rich cores in SCFT composition profiles of diblocks at $\chi N = 40$, $f = 0.29$, and for variable conformational asymmetry (see *SI Appendix*, *3B*. Geometrical *A*nalysis of *S*pherical *D*omains). The first parameter,

$$\alpha_i = \frac{\mathcal{A}_i^{\mathrm{A/B}} - 1}{\mathcal{A}^{\mathrm{poly}} - 1}, \qquad [3]$$

measures the degree of polyhedral warping of the core in terms of the dimensionless area $\mathcal{A}_i^{\mathrm{A/B}}$ of the A/B interface of the i^{th} domain relative to a sphere, where $\mathcal{A}_i^{\mathrm{poly}}$ is the dimensionless area predicted for the perfectly polyhedral interface of the corresponding cell from the unconstrained DFM: $\alpha_i = 0$ for spherical interfaces, and $\alpha_i = 1$ for interfaces that adopt the polyhedral shapes of the DFM cells. We define a second parameter, $\nu(X)$, that measures asymmetry of unequal volumes enclosed within A/B interfaces predicted by SCFT, relative to the volume asymmetry predicted by polyhedral cells of DFM for the same structure X:

$$\nu(X) = \frac{\left\langle \left| \frac{\Delta V_i(X)}{\langle V(X)\rangle} \right|^2 \right\rangle_{\mathrm{A/B}}^{1/2}}{\left\langle \left| \frac{\Delta V_i(X)}{\langle V(X)\rangle} \right|^2 \right\rangle_{\mathrm{poly}}^{1/2}}, \qquad [4]$$

where $\Delta V_i(X) = V_i - \langle V(X)\rangle$ is the volume deviation of the i^{th} domain relative to the average in X and values of $\nu(X)$ greater (less) than 1 indicate that qSD in SCFT are more (less) polydisperse predicted by relaxed DFM cells.

It has been argued previously (27) that the polyhedral warping, or faceting, of core–corona interfaces should increase with ϵ, which controls the ratio of corona- to core-block stiffness, due to the relatively lower entropic cost of more uniformly stretched coronae achieved by polyhedral interfaces. This expectation is consistent with the observed monotonic increase of α from 0 at $\epsilon = 1$ to the saturated value of $\alpha \approx 0.05$ for $\epsilon \gtrsim 2-3$ for the qSD in BCC plotted in Fig. 3*A*.[§] As shown in *SI Appendix*, Fig. S17, the polyhedral warp of the interface grows also with increasing f, due to the increased proximity of the qSD cell boundary to the interface and relatively shorter coronal blocks at larger core fractions. While clearly far from a sharply faceted shape, the increase in core shape anisotropy is obvious from 2D cuts through the qSD shown in Fig. 3*B*, showing a visible warp of A/B interface toward the truncated-octahedral shape of the BCC cell at $\epsilon = 3$.

For the FK phases, which are composed of distinct-symmetry qSD, areal distortion exhibits a markedly different dependence on increased coronal/core stiffness, as illustrated by the plots of α_{12} and α_{14} vs. ϵ for A15 in Fig. 3*C*. Z12 domains exhibit a monotonic, albeit modest, increase in distortion with ϵ. Surprisingly, for the Z14 domains, the excess area drops from its maximal value of $\alpha_{14} \simeq 0.4$ in the conformationally symmetric case for $\epsilon = 1$ down to a lower yet significant plateau value of $\alpha_{14} \simeq 0.2$, roughly twice the areal distortion for BCC.

The origin of this counterintuitive drop in dimensionless area of the Z14 cells with increased outer block stiffness is illustrated in Fig. 3*D*, which compares 2D sections of the Z14 qSD of A15 at $\epsilon = 1$ and $\epsilon = 3$. While the shape for larger outer block stiffness ($\epsilon = 3$) is consistent with a quasi-faceted interface that copies the polyhedral cell (with rounded edges) of the Z14 domain, the conformationally symmetric case ($\epsilon = 1$) is neither faceted nor spherical. It instead adopts oblate or discoidal shape. The contrast in core shape is further reflected in the subinterface (vector) orientational order parameter of A-segments (38) and the spatial distribution of A-block chain ends, also shown in Fig. 3 *D* and *E*. For larger ϵ, the preference for more uniform coronal block stretching drives the quasi-polyhedral domain shape, with radial chain trajectories extending from the center of the domain, a point at which core block ends are concentrated. In contrast, for the case of $\epsilon = 1$, the stiffness of the core blocks is sufficient to resist deformations away from uniform core thickness. Occupying the somewhat flattened Z14 cell with a qSD of uniform core thickness then leads to the discoidal shape, in which chain ends spread laterally in a quasi-lamellar core rimmed by a quasi-toroidal packing at its circumference. The preference for uniform core thickness within the relatively oblate Z14 cell, which gives rise to a larger area discoidal interface for $\epsilon = 1$, ultimately gives way to the quasi-polyhedral qSD shape, and corresponding radial chain stretching, with increased outer block stiffness for $\epsilon \gtrsim 2$ (see schematic in Fig. 3*F*).

SI Appendix, Fig. S18 shows evidence of this same discoidal → polyhedral transition qSD within the most oblate cells of other FK phases, C15 and Z, leading to a corresponding drop in excess area α_i from $\epsilon = 1$ to $\epsilon \approx 2$ for those cells. In Fig. 3*G*, we find this intradomain shape transition with increasing corona-/core-block stiffness is coupled to a transition in volume asymmetry among qSD. Discoidal domains of the conformationally

[§]While this extends beyond what is realized with most flexible linear diblocks, bulky side chains including bottlebrush configurations and miktoarm polymers would make the upper limit accessible.

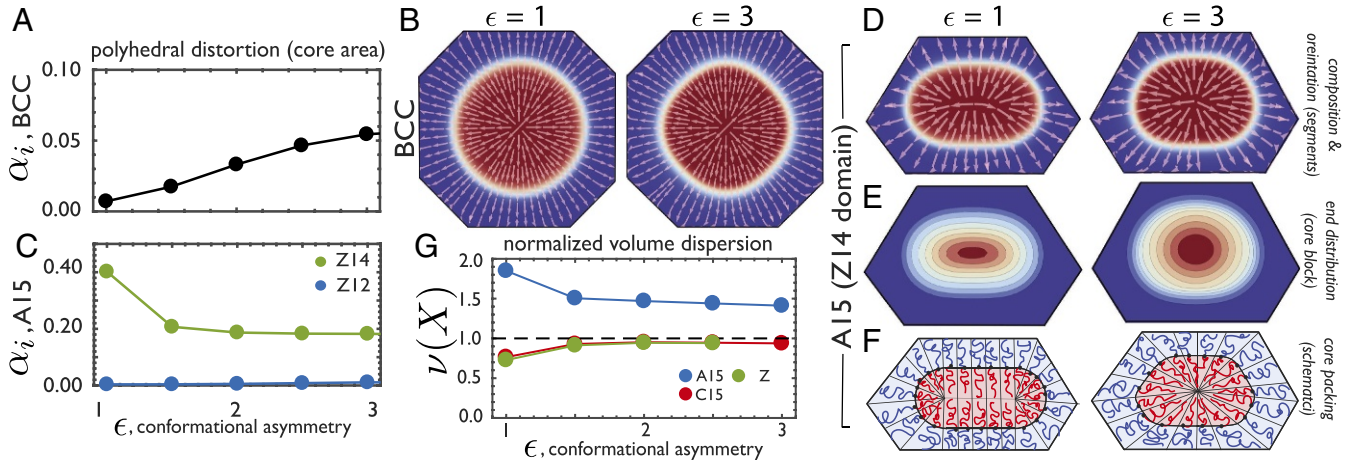

Fig. 3. The polyhedral warping of the A/B interface, measured by α_i from SCFT profiles of $\chi N = 40$ and $f = 0.29$ diblocks, of BCC qSD is plotted vs. conformational asymmetry $\epsilon = a_A/a_B$ in *A*. Corresponding 2D cross-sections (normal to [100] through the center of the primitive cell) of qSD within the truncated-octahedral cells of BCC are shown in *B*, with composition varying from red in A-rich regions to blue in B-rich regions (A/B interface is white). Also shown in vectors are the mean orientation of A-block segments (polar order parameter) (38). In *C*, the areal distortion of Z14 and Z12 qSD from SCFT predictions of A15 is shown (same composition and segregation strength as BCC), with the corresponding section of the Z14 (cut normal to [100] through face of primitive cell, see *SI Appendix*, Fig. S18) qSD shown in *D* as in *B*. Additionally, spatial distribution of the A-block (core forming) chain ends are shown in *E*, varying from zero density (blue) to maximal density (red) within the cores. Schematics illustrating respective discoidal and polyhedral qSD packing are shown in *F*. In *G*, the volume dispersion (normalized by the DFM prediction) is plotted vs. conformational asymmetry.

symmetric diblocks ($\epsilon = 1$) realize a volume dispersion that is strongly divergent from the polyhedral geometry in the DFM, including both greater ($\nu(X) > 1$, for A15) and lesser ($\nu(X) < 1$ for Z, C15) dispersity. However, in the limit of $\epsilon \gtrsim 2$, relatively stiffer coronal blocks pull the cores into radial-stretching, quasi-polyhedral shapes. This transition to more compact cores, in turn, results in volume redistributing among equilibrium qSD tending to the $\nu(X) \to 1$ limit, consistent with agreement between asymmetric volumes of DFM and SCFT shown in Fig. 2*F*.

Notwithstanding the broad agreement between SCFT and DFM predictions, the degree of polyhedral warping of qSD shape is both arguably modest (i.e., $\alpha \lesssim 0.3$ for $\epsilon \gg 1$ for this χN and f) and highly variable in the FK structures, suggesting a heterogeneous degree of shape frustration among cells. Moreover, the discoidal $\to$ polyhedral transition occurs only in high-α qSD, whereas low-α cells (e.g., Z12 cells of A15) maintain radial stretching and a monotonic dependence on ϵ. What controls the variability of coupling between cell geometry of polyhedral distortion? Fig. 4 shows the correlation between α_i for qSD extracted from SCFT at $\chi N = 40$, $f = 0.25$, and $\epsilon = 2$ (i.e., in the quasi-polyhedral shape regime) plotted as a function of the dimensionless stretching $\mathcal{I}_i$ for the corresponding cells from the DFM. The generically increasing trend of α_i with $\mathcal{I}_i$ for cell geometries across competing phases argues that the variable degree of shape frustration within distinct qSD, and its consequent impact on qSD core shape, is regulated by the constraints of asymmetric chain stretching in polyhedral cells. In other words, the ultimate degree of asphericity of core distortion of qSD (measured by dimensionless area) is, in fact, controlled by the local asphericity in radial stretching required by space-filling chain packing (measured by dimensionless radius of gyration).

Concluding Remarks

We anticipate that the emergence of optimal FK lattice structure and thermodynamics via a balance of competing measures of domain asymmetry highlighted here for high-molecular weight diblock copolymers will extend to other copolymer systems where these phases have been observed, including architecturally asymmetric copolymers, linear multiblocks, low-molecular weight/high-χ systems, and blends. In particular, lower molecular weight polymers drive the system closer toward the strong segregation limit and away from the mean-field limit. Each of these materials exhibits different molecular mechanisms through which the relative stiffness of the coronal domain transmits the asymmetry of the local qSD packing into the core shape. For example, the observation of polygonal/polyhedral warping of outer zones of core–shell domains of linear mulitblock polymers (39) provides a plausible mechanism to stabilize the σ phase observed in linear tetrablocks (9). On the other hand, accurately modeling the formation of σ by low-molecular weight conformationally asymmetric diblocks (11, 13) likely requires a non-Gaussian (finite extensibility) model of chain stretching but one that nevertheless, like the dimensionless radius

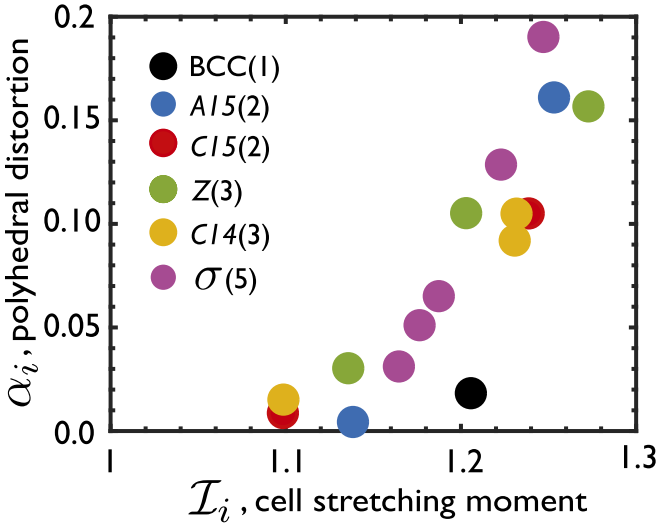

Fig. 4. Correlation between polyhedral warping of core shapes (α_i) within symmetry-distinct qSD extracted from SCFT at $\chi N = 40$, $f = 0.25$, and $\epsilon = 2$ and the degree of frustration of chain stretching in the corresponding cell, quantified by the (cell-wise) dimensionless stretching moment, $\mathcal{I}_i$.

of gyration $\mathcal{I}(X)$, favors compact domains and competes against the minimal area preference for unequal domain volumes. Beyond copolymers, we speculate further that additional intra- and intermolecular mechanisms play the role of balancing the drive for minimal domain area in the formation FK phases, from giant nanotetrahedra (15, 16) to ionic surfactants (17, 18). We speculate that the DFM studied here may anticipate a much broader class of "generalized foam models" that integrate two or more measures of cellular shape and that may be useful as minimal models for a wider range of tessellated architectures (e.g., living tissue) (40).

The present results for the DFM also shed light on the nonequilibrium pathways for stabilizing metastable FK competitors, as has been demonstrated for conformational asymmetric linear diblocks quenched from high-temperature disorder sphere phases to low-temperature metastable, C14, and C15 phases (12, 41). The low-temperature quench is suspected to freeze out the interdomain chain exchange needed to achieve the equilibrium σ state; thus, the kinetically trapped quenched state inherits the volume distribution of the high-temperature micelle liquid state. The DFM suggests a way to analyze the stability of FK states when domain volumes are out of equilibrium, suggesting the observation of C14 and C15 may be selected among the low-temperature kinetically trapped arrangements because it inherits a volume distribution that is both smaller in average cell size and possibly more polydisperse than the equilibrium state at the low temperature and hence a better fit to the "aggregation fingerprint" of low-$\langle Z \rangle$ packings.

ACKNOWLEDGMENTS. We are grateful to R. Gabbrielli and J.-F. Sadoc, R. Mosseri for valuable input on geometric models of cellular packings, as well as to A.-C. Shi, M. Mahanthappa, and A. Travesset for additional discussion. This research was supported by Air Force Office of Scientific Research under Asian Office of Aerospace Research and Development Award 151OA107 and National Science Foundation Grants DMR-1719692 and DMR-1359191 (Research Experiences for Undergraduates Site: B-SMaRT). G.M.G. also acknowledges the hospitality of the Aspen Center for Physics, supported by NSF Grant PHY-1607611, where some of this work was completed. SCFT calculations were performed using computational facilities at the Massachusetts Green High Performance Computing Center and the Minnesota Supercomputing Institute.

1. Hyde S, et al. (1997) *The Language of Shape: The Role of Curvature in Condensed Matter: Physics, Chemistry and Biology* (Elsevier, Amsterdam).
2. Frank FC, Kasper JS (1959) Complex alloy structures regarded as sphere packings. II. Analysis and classification of representative structures. *Acta Cryst* 12: 483–499.
3. Shoemaker DP, Shoemaker CB (1986) Concerning the relative numbers of atomic coordination types in tetrahedrally close packed metal structures. *Acta Cryst* 42: 3–11.
4. Nelson DR, Spaepen F (1989) Polytetrahedral order in condensed matter. *Solid State Phys* 42:1–90.
5. Sadoc JF, Mosseri R (2000) *Geometrical Frustration* (Cambridge Univ Press, Cambridge).
6. Travesset A (2017) Nanoparticle superlattices as Quasi-Frank-Kasper phases. *Phys Rev Lett* 119:115701.
7. Balagurusamy VSK, Ungar G, Percec V, Johansson G (1997) Rational design of the first spherical supramolecular dendrimers self-organized in a novel thermotropic cubic liquid-crystalline phase and the determination of their shape by x-ray analysis. *J Am Chem Soc* 119:1539–1555.
8. Zeng X, et al. (2004) Supramolecular dendritic liquid quasicrystals. *Nature* 428:157–160.
9. Lee S, Bluemle MJ, Bates FS (2010) Discovery of a Frank-Kasper sigma phase in sphere-forming block copolymer melts. *Science* 330:349–353.
10. Chanupriya S, et al. (2016) Cornucopia of nanoscale ordered phases in sphere-forming tetrablock terpolymers. *ACS Nano* 10:4961–4972.
11. Lee S, Leighton C, Bates FS (2014) Sphericity and symmetry breaking in the formation of Frank-Kasper phases from one component materials. *Proc Natl Acad Sci USA* 50:17723–17731.
12. Kim K, et al. (2017) Thermal processing of diblock copolymer melts mimics metallurgy. *Science* 330:349–353.
13. Schulze MS, et al. (2017) Conformational asymmetry and quasicrystal approximants in linear diblock copolymers. *Phys Rev Lett* 118:207801.
14. Cho BK, Jain A, Gruner SM, Wiesner U (2004) Mesophase structure-mechanical and ionic transport correlations in extended amphiphilic dendrons. *Science* 305:1598–1601.
15. Huang M, et al. (2015) Selective assemblies of giant tetrahedra via precisely controlled positional interactions *Science* 348:424–428.
16. Yue K, et al. (2016) Geometry induced sequence of nanoscale Frank-Kasper and quasicrystal mesophases in giant surfactants. *Proc Natl Acad Sci USA* 113:14195–14200.
17. Kim SA, Jeong KJ, Yethiraj A, Mahanthappa MK (2017) Low-symmetry sphere packings of simple surfactant micelles induced by ionic sphericity. *Proc Natl Acad Sci USA* 114:4072–4077.
18. Baez-Cotto CM, Mahanthappa MK (2018) Micellar mimicry of intermetallic C14 and C15 laves phases by aqueous lyotropic self-assembly. *ACS Nano* 12:3226–3234.
19. Hajiw S, Pansu B, Sadoc JF (2015) Evidence of C14 Frank-Kasper phase in one-sized gold nanoparticle superlattices. *ACS Nano* 9:8116–8121.
20. Weaire D, Phelan R (1994) The structure of monodisperse foam. *Phil Mag Lett* 70:345–350.
21. Phelan R (1996) Generalizations of the Kelvin problem and other minimal problems. *The Kelvin Problem*, ed Weaire D (Taylor & Francis, London), pp 125–139.
22. Kusner R, Sullivan JM (1996) Comparing the Weaire-Phelan equal-volume foam to Kelvin's foam. *Forma* 11:233–242.
23. Cox SJ, Graner F, Mosseri R, Sadoc JF (2017) Quasicrystalline three-dimensional foams. *J Phys Condens Matter* 29:114001–114010.
24. Ziherl P, Kamien RD (2000) Soap froths and crystal structures. *Phys Rev Lett* 16:3528–3531.
25. Ziherl P, Kamien RD (2001) Maximizing entropy by minimizing area: Towards a new principle of self-organization. *J Phys Chem B* 105:10147–10158.
26. Grason GM, DiDonna BA, Kamien RD (2003) Geometric theory of diblock copolymer phases. *Phys Rev Lett* 91:058304.
27. Grason GM (2006) The packing of soft materials: Molecular asymmetry, geometric frustration and optimal lattices in block copolymer melts. *Phys Rep* 443:1–64.
28. Xie N, Li W, Qiu, F, Shi AC (2014) σ phase formed in conformationally asymmetric AB-type block copolymers. *ACS Macroletters* 3:906–910.
29. Iacovella CR, Keys AR, Glotzer SC (2011) Self-assembly of soft-matter quasicrystals and their approximants. *Proc Natl Acad Sci USA* 108:20935–20940.
30. Conway JH, Sloane NJA (1988) *Sphere Packings, Lattices and Groups* (Springer-Verlag, New York), Chap 2.
31. Matsen MW (2002) The standard Gaussian model for block copolymer melts. *J Phys Condens Matter* 14:R21–R47.
32. Arora A, et al. (2016) Broadly accessible self-consistent field theory for block polymer materials discovery. *Macromolecules* 49:4675–4690.
33. Olmsted PD, Milner ST (1994) Strong-segregation theory of bicontinuous phases in block copolymers. *Phys Rev Lett* 72:936–939.
34. Olmsted PD, Milner ST (1998) Strong-segregation theory of bicontinuous phases in block copolymers. *Macromolecules* 31:4011–4022.
35. Grason GM, Kamien RD (2005) Interfaces in diblocks: A study of miktoarm star copolymers. *Macromolecules* 37:7371–7380.
36. Du Q, Faber V, Gunzburger M (1999) Centroidal Voronoi tessellations: Applications and algorithms. *SIAM Rev* 41:637–676.
37. Brakke KA (1992) The surf evolver. *Exp Math* 1:141–165.
38. Prasad I, Seo Y, Hall LM, Grason GM (2017) Intradomain textures in block copolymers: Multizone alignment and biaxiality. *Phys Rev Lett* 118:247801.
39. Gido SP, Schwarz DW, Thomas EL, Goncalves M (1993) Observation of a non-constant mean curvature interface in an ABC triblock copolymer. *Macromolecules* 26:2636–2640.
40. Kaliman K, Jayachandran C, Rehfeldt F, Smith A-S (2016) Limits of applicability of the Voronoi tessellation determined by centers of cell nuclei to epithelium morphology. *Front Physiol* 7:551.
41. Kim K, et al. (2017) Origins of low-symmetry phases in asymmetric diblock copolymer melts. *Proc Natl Acad Sci USA* 115:847–854.